Using Fan Depressurization Test Data in Building Detailed Air Flow Network Models: Approach and Impacts

Adam D. Wills[1], Justin Berquist[1], Iain A. Macdonald[1], Carsen Banister[1]
[1]National Research Council Canada, Ottawa, Canada

Abstract

Building envelope and HVAC minimum performance requirements continue to increase in building regulations to meet ambitious energy and emissions reductions targets. Therefore, envelope airtightness is an increasingly significant determinant of building performance. The 2015 National Building Code of Canada (NBC) enables home builders to obtain optional credits for airtight design by performing a fan depressurization test and using the results in building performance simulation. The simplified empirical Alberta Infiltration Model (AIM-2) is typically used in the NBC to simulate small building infiltration, which directly uses fan test results. This paper describes the application of airflow network (AFN) models for simulating small building infiltration. An approach for using typical blower door depressurization data in AFNs is proposed, and a series of scenarios are used to benchmark model estimates against AIM-2. AFN models are then used to analyze the sensitivity of annual building performance to leakage site vertical and orientation distribution.

Introduction

Building codes around the world are being leveraged to improve energy performance and reduce greenhouse gas emissions in the building sector. The typical mechanism used is to increase the minimum thermal performance of envelope components and minimum efficiency of mechanical systems. Subsequently, these components contribute a smaller portion of the building system energy consumption and losses, making envelope infiltration an increasingly dominant determinant of overall building performance.

Canada currently publishes energy provisions in two model building codes: the National Building Code (NBC) (CCBFC, 2015), and the National Energy Code for Buildings (NECB) (CCBFC, 2017). The NECB is typically applied to large commercial buildings; Section 9.36 of the NBC provides the minimum energy performance for housing and small buildings.

For both the NBC and NECB, codes energy performance compliance may be demonstrated using two pathways: prescriptive and performance. The prescriptive path requires builders to demonstrate that mechanical and envelope components meet minimum prescribed performance levels. The performance path requires energy calculations or simulations to demonstrate that a building performs as well or better than a code reference building. This calculation is often accomplished using building performance simulation (BPS) tools. Modelling of thermal energy flow through envelope components and mechanical systems is well-established and understood; however, the modelling of envelope infiltration in whole-building BPS continues to be simplified.

Current Infiltration Models in Code

The NECB currently assumes a constant flow rate of 0.25 L/s per m^2 of total gross above-ground wall and roof areas to model infiltration for the performance compliance path. The NBC implicitly requires the use of empirical infiltration models such as the Sherman-Grimsrud Model (Sherman & Grimsrud, 1980) or the Alberta Infiltration Model (AIM-2) (Walker & Wilson, 1990) to demonstrate performance path compliance. These models use the results of fan depressurization tests to model total envelope infiltration, Q_{inf} [m^3/s], under operating conditions. AIM-2 represents total envelope leakage using a power law:

$$Q_{inf} = C(\Delta P)^n \quad (1)$$

where C [m^3/(s·Pa^n)] and n [-] are the flow coefficient and exponent, respectively, which are determined from regressing fan depressurization test results, and ΔP [Pa] is the pressure difference across the envelope.

By assuming the flow coefficient n is equal for all leakage sites in the envelope, the flow coefficient C is distributed across the envelope using the expression:

$$C = C_c + C_f + C_w + C_{flue} \quad (2)$$

where C_c, C_f, C_w, and C_{flue} are the flow coefficients for the leakage sites at the ceiling, floor, wall, and flue, respectively. The user must specify how C is distributed across the coefficients on the right hand side of Equation 2. AIM-2 also assumes that all four walls have uniformly distributed leakage.

Wind-effect infiltration, Q_w [m^3/s], is determined from:

$$Q_w = C \cdot f_w \cdot P_w^n \quad (3)$$

where f_w is the wind factor and P_w [Pa] is the reference wind pressure:

$$P_w = \rho_o \frac{(S_w U_e)^2}{2} \quad (4)$$

where S_w is a static local wind shelter coefficient, U_e [m/s] is the unobstructed wind speed at the eaves height, and ρ_o [kg/m^3] is the outdoor air density.

The wind factor is determined from:

$$f_w = 0.19(2-n)\left[1 - \left(\frac{X+R}{2}\right)^{\left(\frac{3}{2}\right)}\right] \quad (5)$$

where:

$$X = \frac{C_c - C_f}{C} \quad (6)$$

$$R = \frac{C_c + C_f}{C} \quad (7)$$

Walker & Wilson (1990) derived Equation 5 using the wind tunnel test data from Akins et al. (1979) for square footprint buildings and wind normal to the upwind wall. It can be seen from Equations 3 to 7 that the AIM-2 wind-effect infiltration calculation is implicitly independent of wind direction.

Stack-effect infiltration, Q_s [m^3/s], is determined from:

$$Q_s = C \cdot f_s \cdot P_s^n \quad (8)$$

where P_s [Pa] is the stack-effect pressure:

$$P_s = \rho_o \cdot g \cdot H \cdot \left(\frac{T_i - T_o}{T_i}\right) \quad (9)$$

where ρ_o [kg/m^3] is the outdoor air density, g [m/s^2] is gravitational acceleration, H [m] is the height of the building eaves, and T_o [K] is the outdoor air temperature.

The stack flow factor, f_s, is determined in AIM-2 as:

$$f_s = \left(\frac{1+n\cdot R}{n+1}\right) \cdot \left[\frac{1}{2} - \frac{1}{2} \cdot \left(\frac{X^2}{2-R}\right)^{5/4}\right]^{n+1} \quad (10)$$

Wilson & Walker (1990) stated the functional form of Equation 10 is an approximation selected to produce correct model behaviour at the limits of X and R.

Advanced Infiltration Modelling Approaches

According to Clarke (2001), air flow modelling approaches from simplest to most complex are: scheduled, empirical, air flow networks (AFNs), and computational fluid dynamics (CFD). Scheduled flow is what is currently used by the NECB; a fixed flow of outdoor air is defined as a function of envelope area. Flow rate may also vary based on a schedule to simulate aspects of building use, such as the opening of windows. AIM-2 is an empirical infiltration methodology which uses measured data to simulate envelope infiltration under operating conditions.

In the context of annual whole-building energy simulation, CFD is typically too computationally intensive and the relatively large quantity of model inputs may be difficult or impossible to define, especially at early design stages.

AFN models bridge the gap between empirical and CFD models. The modelling approach represents building air flow using a network of pressure nodes linked by flow inducers (fans) or inhibitors (cracks, windows, etc.). The nodes are either boundary (wind-induced or user-specified) or internal with known or unknown pressure. The internal nodes nominally represent a well-mixed volume of air. The model is steady-state based Bernoulli's equation, and typically computed at sub-hourly timescales. Each flow path needs to be explicitly defined which is non-trivial; however, the system of equations to be solved are several orders of magnitude smaller than CFD, and AFNs can provide greater insight on the pathways of energy and mass flow through buildings compared to empirical approaches.

Objectives

The purpose of this study was to answer two questions:

1. Can an AFN be used to model fan depressurization test results, and how does it compare with a validated empirical model?
2. Using the detailed AFN model, how sensitive is annual energy performance variations in leakage site elevation and directional distributions?

Methodology

Several BPS tools offer a variety of models to simulate infiltration and air flow in buildings. For this study the simulation tool ESP-r v13.3.13 (Clarke J. A., 2021) was used. ESP-r has the capability to model air flow using all approaches mentioned previously. Empirical infiltration is modelled using AIM-2. The AFN modelling approach used in ESP-r is described by Hensen (1991).

Architecture of ESP-r

ESP-r uses a collection of specialized solvers to separately model heat and mass transfer, and other building performance domains such as daylighting. The transient thermal solver uses a finite-difference discretization to solve the transient heat flow through the envelope and internal air volumes. The air nodes in the thermal zone are linked to air nodes in the air flow domain which receive temperature from the thermal solver to resolve flow within the defined air flow network or model.

The AFN solver can be coupled to the finite interior volumes of the thermal domain, and are represented by a single pressure node. The nodes are connected to each other and boundary nodes to form the AFN and solve the airflow at each timestep. The determined air flows are then passed back to the thermal domain as an equivalent thermal energy conductance into or out of the thermal zone. Further details are omitted here for clarity, and the interested reader is directed to Clarke (2001) for additional information.

AIM-2 and AFN models are implemented in ESP-r as separate solvers, and independently interact with the thermal domain solver.

Case Study Building

A case study building is used here to describe the methodology for generating an AFN model that produces comparable infiltration estimates to AIM-2, and is defined using fan depressurization test results. The Indoor Air Research Laboratory (IARL) located in Ottawa, Canada,

was used as the case study building. This facility is a two-storey building, shown in Figure 1.

Figure 1: IARL facility in Ottawa, Canada.

The IARL is equipped with a dedicated air handling unit and motorized dampers which control air flow to each room. The silver discs seen in Figure 1 are envelope leakage ports. The facility contains 32 individually controlled ports that may be actuated to alter envelope leakage site size and location. The exterior walls have an effective thermal resistance of 4.13 m^2·K/W and ceilings below attic are 7.20 m^2·K/W. The discretized ESP-r model is shown in Figure 2.

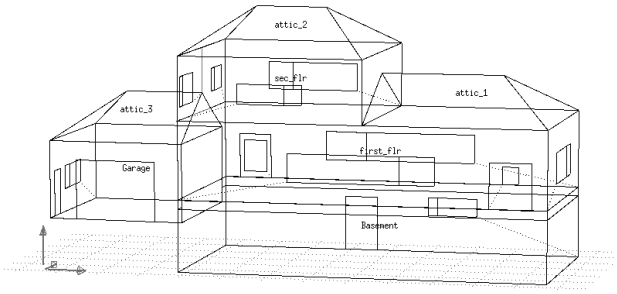

Figure 2: ESP-r model of the IARL.

The interior conditioned space is divided into three air nodes representing the basement, first, and second floor spaces and has a total volume of 1424 m^3. Additional unconditioned zones include three attic spaces and an attached garage.

Developing the infiltration AFN model

AIM-2 uses several assumptions in order to utilize fan depressurization data to model infiltration:

- The flow exponent for each leakage site is the same as the whole-building measured exponent;
- The wind-induced pressure coefficient for the attic is the weighted average of soffit, gable vents, and roof vent boundary pressure coefficients;
- The wind factor, f_w, expression in Equation 5 was derived from test results for a square floorplan building;
- f_w is implicitly independent of wind direction and was derived assuming wind normally incident on one side.

AIM-2 also only returns the total infiltration rate for all tested/conditioned spaces. In the ESP-r implementation of the model, the user specifies which zones receive the infiltration and which zone temperature, T_i, is used to determine the stack effect reference pressure, P_s. Once AIM-2 calculates the whole-building infiltration, the flow is distributed on a volume-weighted basis to the linked zones.

The AFN infiltration model developed for this study is depicted in Figure 3.

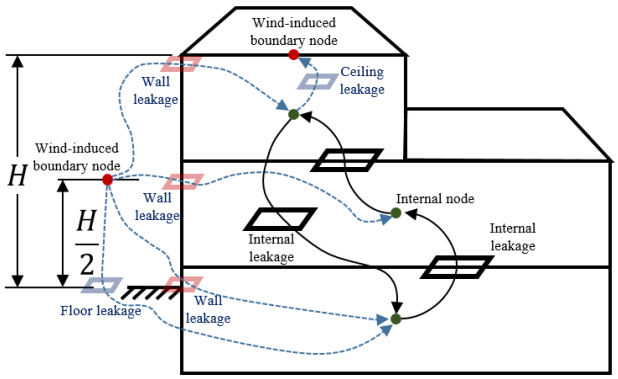

Figure 3: AFN developed for the IARL.

One wind-induced boundary pressure node was defined for each façade direction at an elevation equal to $H/2$. For each façade, three leakage sites were defined and distributed at vertical elevations of $z = 0$, $z = H/2$, and $z = H$. Leakage was characterized using a flow inhibitor component which uses the same form as Equation 1. These leakage sites are intended to be analogous to the average "wall" leakage in AIM-2.

A single wind-induced boundary node, at an elevation equal to H, and single leakage path was used to define ceiling/attic leakage. The floor leakage was characterized by duplicating each of the four lowest elevation leakage connections defined previously for the wall. Floor and ceiling leakage paths were also characterized using a flow inhibitor component.

The interior nodes are also connected via generic opening components. This is to simulate the inter-zonal air exchange that occurs within the building. Per Hensen (1991), the flow through this component, $\dot{m}_{comp}$ [kg/s], is characterized as:

$$\dot{m}_{comp} = 0.65 \cdot A_{comp} \cdot \sqrt{2 \cdot \rho \cdot \Delta P} \qquad (11)$$

where A_{comp} [m^2], is the area of the opening, ρ [kg/m^3] is the density of the air entering the component, and ΔP [Pa] is the pressure difference across the component. An A_{comp} of 10 m^2 was selected as being appropriate for free movement of air between the interior nodes.

Like AIM-2, the user must define the fraction of leakage between floor, wall, and ceiling, and thus define C_f, C_w, and C_c. To acknowledge assumptions in AIM-2, the leakage is equally distributed across all sides, and for wall leakage evenly across all elevations on each side; i.e., the leakage component for each of the twelve wall surfaces has a flow coefficient equal to $C_w/12$.

Another input that needs to be defined is the pressure coefficients, $C_{p,i,d}$, for the AFN boundary nodes which

relate wind speed to wind-induced pressure at the i^{th} building surface, P_i [Pa] (Hensen, 1991):

$$P_i = \frac{1}{2} \cdot C_{p,i,d} \cdot \rho \cdot U_r^2 \qquad (12)$$

where ρ is the air density [kg/m^3], and U_r [m/s] is the wind speed at reference height r and direction d measured from the surface normal. To align with AIM-2, the set of pressure coefficients for a square footprint building from Akins et al. (1979) was used. These pressure coefficients represents the average wall surface pressure relative to wind speed at eaves height; therefore, $U_r = U_e$. Figure 4 plots $C_{p,i,d}$ versus wind angle, with 0° indicating wind direction normal toward the surface.

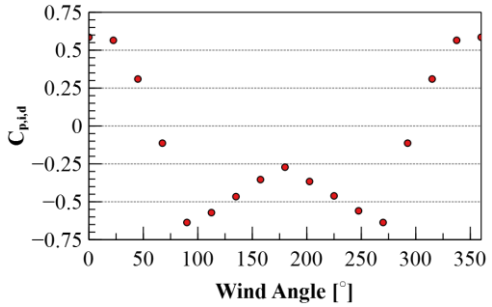

Figure 4: Surface pressure coefficients, data from Akins et al. (1979).

U_e was determined from meteorological wind speed, U_{met}, using (Bradley & Riley, 1993):

$$U_e = U_{met} \cdot \frac{\ln\left(\frac{60}{Z_{met}}\right) \cdot \ln\left(\frac{H}{Z_{site}}\right)}{\ln\left(\frac{H_{met}}{Z_{met}}\right) \cdot \ln\left(\frac{60}{Z_{site}}\right)} \qquad (13)$$

where Z_{met} and Z_{site} [m] are the terrain roughness lengths of the meteorological and building sites, respectively, and H_{met} is the height the wind observations were measured at.

A constant pressure coefficient of -0.56 (does not vary with wind direction) was defined for the wind-induced ceiling/attic boundary node. This value was derived from the weighted average of the pressure coefficients at the eaves height of each wall (each weighted 0.125), and the roof (0.5 weight) of a rectangular building as reported by Akins et al. (1979) when wind is normal to one side. This weighting assumes leakage area of eaves is evenly distributed on each side, and sum of eave leakage area is equal to roof leakage area.

Simulation Plan

Initial comparisons between AIM-2 and the proposed AFN infiltration modelling approach used four climate scenarios:

1. Climate Zone 5 (3000≤HDD$_{18}$<3999), low wind;
2. Climate Zone 5, high wind;
3. Climate Zone 8 (HDD$_{18}$≥7000), low wind;
4. Climate Zone 8, high wind.

Warmer and colder climates were selected to capture extreme stack-effect boundary conditions, and high and low wind for extreme wind-effect boundary conditions. The locations were selected using the wind resource map from Canadian Geographic (2009) and the HDD$_{18}$ values reported in the NECB are:

1. Nakusp, BC (Scenario 1, HDD$_{18}$=3560);
2. Toronto, ON (Scenario 2, HDD$_{18}$=3520);
3. Dawson, YK (Scenario 3, HDD$_{18}$=8120);
4. Yellowknife, NT (Scenario 4, HDD$_{18}$=8170).

The hourly annual Canadian weather year for energy calculations (CWEC) data from ECCC (2021) were used in the simulations. The annual wind conditions reported in the CWEC files for each of the locations are summarized in the sorted ascending wind speed plot in Figure 5:

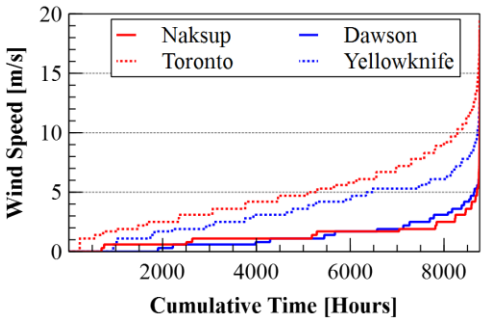

Figure 5: Annual hourly wind speeds for selected locations, sorted ascending.

Figure 5 is interpreted the same way as a load duration curve; e.g. for 6000 hours the wind in Toronto is 5.8 m/s or less. It can be seen in Figure 5 that Toronto and Yellowknife have higher wind speeds for longer durations compared to Naksup and Dawson.

The whole-building envelope leakage of the building was set to 2.5 ACH @ ΔP = 50 Pa with $n = 0.67$. This is the implicit reference envelope airtightness used in Section 9.36 of the 2015 NBC. For both AIM-2 and AFN models, the meteorological and building site terrains were set to "open sea" ($Z_{site} = Z_{met} = 0.0002$ m) (Bradley & Riley, 1993). No local shielding was assumed for both models.

Table 1 summarizes the leakage distribution simulations considered using each climate and infiltration model for the AIM-2 and AFN inter-model comparison.

Table 1: Leakage fraction elevation distribution scenarios.

Scenario #:	**1**	**2**	**3**	**4**	**5**	**6**	**7**
Ceiling	0.33	0.49	***0.02***	0.49	0.98	***0.01***	***0.01***
Wall	0.34	***0.02***	0.49	0.49	***0.01***	***0.01***	0.98
Floor	0.33	0.49	0.49	***0.02***	***0.01***	0.98	***0.01***

The scenarios cover even distribution across the elevations and concentration of leakage at one or two elevations. Near zero values, in red bold italics, were used in Table 1 to represent zero for mathematical solution purposes.

Each scenario was simulated using AIM-2 and the AFN model over an annual period at a five minute timestep. Infinite capacity ideal convective heating and cooling was modelled with setpoints of 21 and 25 °C, respectively, in the three occupied zones. The ideal control in ESP-r solves

required space heating or cooling flux to precisely maintain the zone within the bounds of the setpoints.

The second set of simulations used the Toronto climate data to analyse the sensitivity of leakage site orientation to AFN model annual modelled infiltration and energy consumption. Figure 6 plots the wind rose for the Toronto CWEC climate. The radial units are cumulative hours of the year. It can be seen that over the year the wind largely originates from the west and north 70° east.

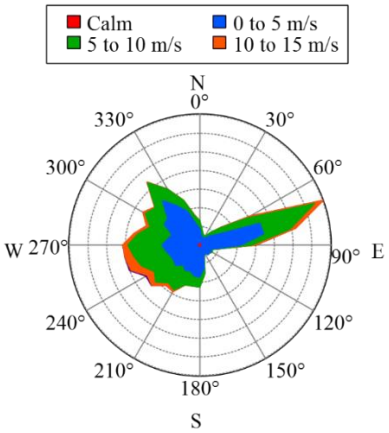

Figure 6: Wind rose for Toronto CWEC climate data.

All scenarios in the second set assumed wall-only leakage (as per Scenario 7 in Table 1), and at each elevation on the wall the orientation distribution of the leakage was varied. The leakage values for opposite wall orientation exposures are assumed to be equal as this yields highest wind-driven infiltration through the building. The second set of scenarios considered is summarized in Table 2:

Table 2: Leakage fraction orientation distribution scenarios.

	1	**2**	**3**	**4**
North-South	0.01	0.25	0.75	0.99
East-West	0.99	0.75	0.25	0.01

In Scenario 1, for example, 49.5% of the total building leakage is facing east, 49.5% is facing west, and the remaining 1% is divided evenly between north and south. The same simulation period and controls were used as the first set of simulations.

Results

The results are divided into two sections. The first section describes the results of the AIM-2 and AFN model comparison simulations which considered the scenarios described in Table 1. The second section presents the results of the study varying orientation of leakage sites for the Toronto climate and scenarios described in Table 2.

Comparing AIM-2 and AFN Model

To compare the performance of the models, the estimated infiltration, expressed as air changes per year (ACY), was calculated for each climate, scenario, and infiltration model and are plotted in Figure 7. Figure 8 plots the percentage difference in ACY infiltration estimates between AIM-2 and the AFN infiltration model, where a positive value indicates higher ACY estimates using AIM-2, and a negative value indicates higher infiltration when the AFN model is used.

Both figures show good agreement between the AFN model and AIM-2. The absolute difference of annual infiltration estimates between models ranges from 4 to 288 ACY across all climates and scenarios which is equivalent to a constant 0.0004 to 0.0328 air changes per hour (ACH) for a full year. The AFN model yielded higher ACY estimates for 16 of the 28 scenarios. The largest percentage difference occurs in Scenario 5 when all leakage is concentrated at the ceiling, with the AFN yielding higher leakage estimates. However, these large percentage differences are due to the relatively small magnitudes of ACY estimates from both models in that scenario. The absolute difference in annual infiltration estimates for scenario 5 were found to be 46 to 74 ACY across all climates.

Figure 7 further shows that better agreement between AIM-2 and the AFN model is achieved in the low wind climates (Nakusp and Dawson) compared to the high wind climates (Toronto and Yellowknife). The absolute difference in ACY model estimates ranges between 4 and 109 ACY with a median of 51 ACY across the low wind climates and all scenarios, and 10 to 288 ACY with a median of 137 ACY across the high wind climates and all scenarios.

Temporal differences in infiltration estimates between AIM-2 and the AFN model for each simulation timestep were analysed using the coefficient of the variation of the root mean square error (CV(RMSE)), normalized mean bias error (NMBE), and the mean absolute error (MAE) of whole-building infiltration ACH estimates, with AIM-2 estimates used as the "observed" variables. Tables 3 and 4 provide the summary of these comparator metrics for the warm and cold climate simulations, respectively. MAE is reported in thousandths (10^{-3}) of ACH units for convenience; i.e., 0.6 in the table is 0.0006 ACH.

The impact of the different scenarios and infiltration models on annual space heating and cooling demands are summarized in Figures 9 and 10. The distribution of annual heating demands in Figure 9 follow the infiltration estimate trends seen in Figure 7, where higher estimates of infiltration yield higher estimates of heating demand. Absolute differences in model estimates of annual space demand range from 0.2 to 15 GJ/year with a median of 3.1 GJ/year. The largest difference is observed for Yellowknife in Scenario 3 where leakage is evenly divided between the wall and floor (no ceiling leakage).

Table 3: Temporal difference metrics for warm climate simulations.

	Scenario						
Nakusp	**1**	**2**	**3**	**4**	**5**	**6**	**7**
CV(RMSE) [%]	5	5	13	10	187	12	12
NMBE [%]	-3	-2	8	-8	-175	2	-6
MAE [ACH·10^3]	4.6	3.6	8.9	9.0	5.3	0.8	6.0
Toronto	**1**	**2**	**3**	**4**	**5**	**6**	**7**
CV(RMSE) [%]	7	14	13	16	80	14	12
NMBE [%]	-3	-9	9	-12	-70	8	8
MAE [ACH·10^3]	7.0	21.3	27.9	26.0	6.2	22.9	22.9

Absolute differences in space cooling demand estimates range from 0.0 to 2.0 GJ/year with a median of 0.2 GJ/year. The largest differences are all in Scenario 6 (all leakage concentrated at the floor) for each climate.

Table 4: Temporal difference metrics for cold climate simulations.

	Scenario						
Dawson	**1**	**2**	**3**	**4**	**5**	**6**	**7**
CV(RMSE) [%]	5	8	11	7	195	15	10
NMBE [%]	0	3	7	-5%	-179	-1	-5
MAE [ACH·10^3]	0.6	5.7	12.5	8.1	7.6	0.4	7.3
Yellow-knife	**1**	**2**	**3**	**4**	**5**	**6**	**7**
CV(RMSE) [%]	6	8	17	11	131	14	12
NMBE [%]	0	-2	13	-8	-120	8	5
MAE [ACH·10^3]	1.1	4.6	32.8	17.7	8.5	13.7	13.5

Varying Leakage Site Orientation

Figure 11 plots the annual infiltration and space heating demand estimates for the scenarios described in Table 2. Also included in the plot is Scenario 7 from Table 2, labeled as 'Base', where leakage sites are evenly distributed across all orientations.

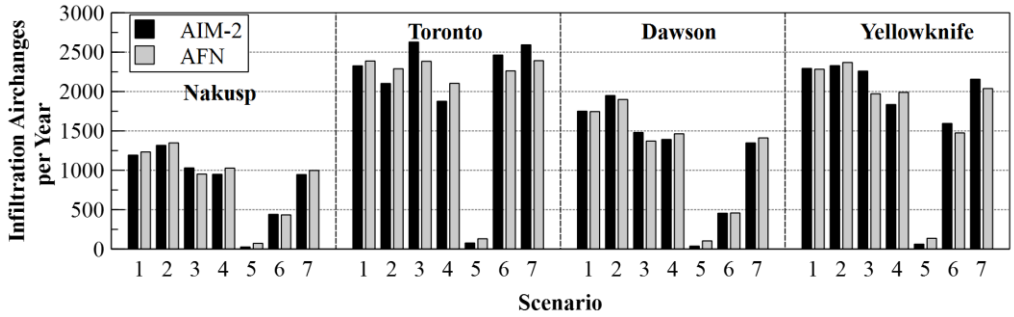

Figure 7. Annual infiltration for different climates, infiltration models, and leakage distribution scenarios.

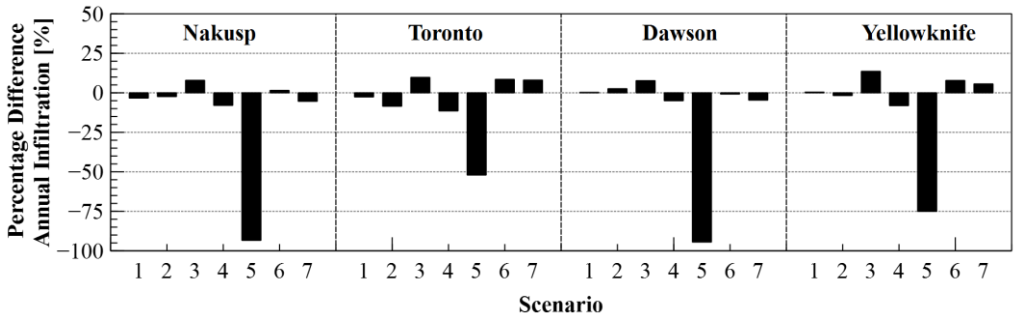

Figure 8: Percentage difference of annual infiltration estimates between AIM-2 and AFN.

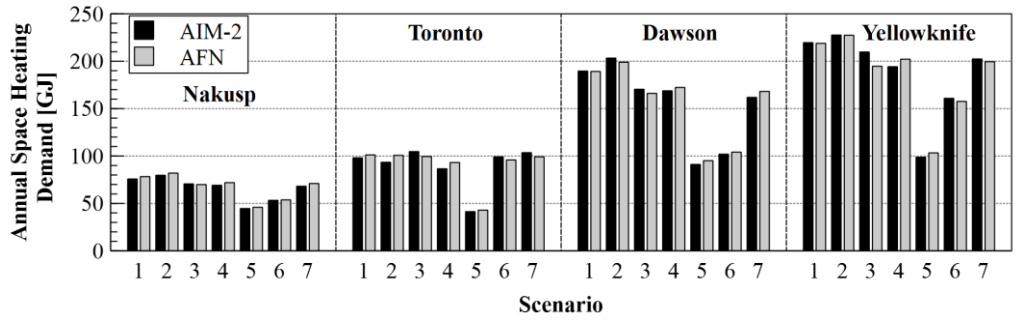

Figure 9: Annual space heating demand for different climates, infiltration models, and leakage distribution scenarios.

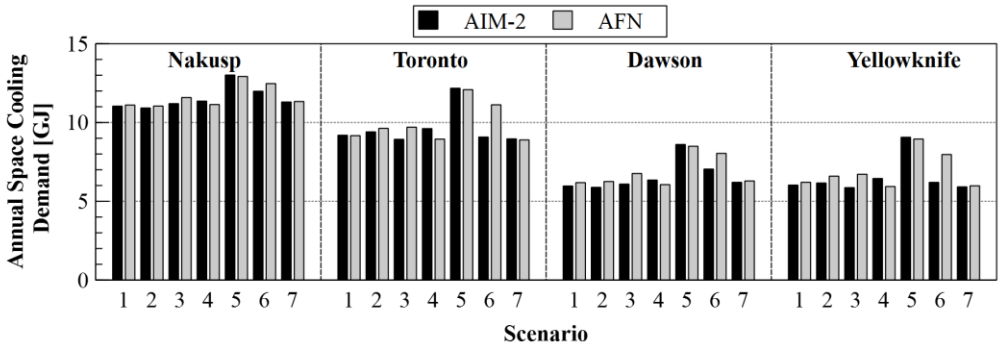

Figure 10: Annual space cooling demand for different climates, infiltration models, and leakage distribution scenarios.

Scenarios 1 and 2 in Figure 11, which orient envelope leakage toward the dominant wind direction in the climate, are shown to have the highest infiltration and space heating demand whereas Scenarios 3 and 4, which orient leakage parallel to the dominant wind direction, have the lowest.

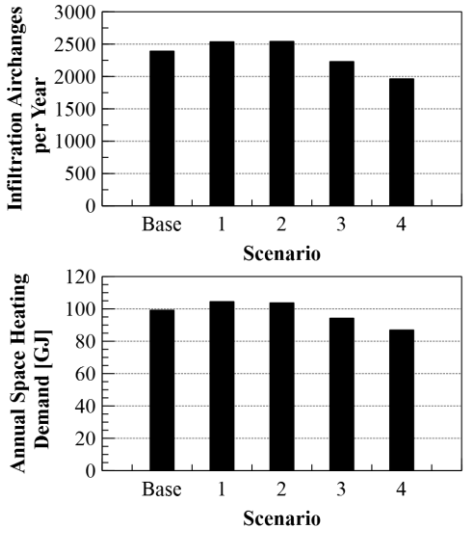

Figure 11: Annual infiltration and space heating demand for the leakage site orientation scenarios.

Relative to the base case (leakage evenly distributed in all orientations), Scenario 2 increased annual infiltration and space heating demand estimates by 6% and 5%, respectively. Scenario 4 decreased annual infiltration and space heating demand estimates by 18% and 12%, respectively.

Discussion

The results presented in Figures 8 to 11 demonstrate that when similar boundary conditions and assumptions as AIM-2 are applied to an AFN infiltration model, similar annual infiltration, space heating, and space cooling estimates can be achieved across a variety of leakage distribution and climate scenarios. With the exception of Scenario 5 in Table 1 (all leakage at the ceiling), CV(RMSE) between AFN and AIM-2 infiltration estimates range from 5% to 17%. NMBE between the models (also excluding Scenario 5), ranges from 0% and 13%. ASHRAE Guideline 14 (ASHRAE, 2014) uses limits of 10% and 30% for CV(RMSE) and NMBE , respectively, for acceptable agreement between measured and calibrated model hourly data. Based on these criteria and the fact the CV(RMSE) and NMBE values were calculated here using five-minute timestep data, Tables 3 and 4 show good agreement between the AFN and AIM-2 models. Since AIM-2 was previously validated using SF_6 tracer gas infiltration measurements of two research houses (Walker & Wilson, 1990), the inter-model comparison conducted here lends validity to the modelling approach proposed.

Scenario 5 in Table 1 was shown to have the largest CV(RMSE) and NMBE values in all climates; however, the mean absolute error (MAE) of the leakage estimates is comparable to the MAE values observed in the other leakage scenarios. The relatively low infiltration rates in this leakage scenario, seen in Figure 7, increases the relative normalized differences between the models compared to the higher infiltration rates observed in the other leakage scenarios. Scenario 5 has the lowest infiltration since leakage is concentrated at a single elevation removing stack effect flow. There is also limited wind-effect infiltration since, as can be seen using Figure 3, there is only one path into and out of the conditioned space through the ceiling limiting infiltration to pass through the conditioned space. It can be shown using Equations 5 to 10 that the wind and stack factors in AIM-2 equate to zero when all leakage is at the ceiling.

Another notable observation is the difference in annual cooling demands in Scenario 6 (all leakage at the floor) in Figure 10. Using Figure 3, it can be seen that during the cooling season, outdoor infiltration is all passed to the basement node in the AFN model. Thermal stratification and no leakage paths above the basement inhibits mixing of outdoor air with the other zones. Therefore, without the free cooling from outdoor air, the main and second floors require additional space cooling from the space conditioning system. Recall that the AIM-2 implementation in ESP-r calculates whole-building infiltration and distributes it on a volume-weighted basis. Thus, AIM-2 provides relatively

more outdoor air and free cooling to the above-grade zones in this scenario. This observation highlights the potential of AFN to better characterize the zonal impacts of infiltration compared to the whole-building calculation approach in AIM-2.

The second set of scenarios in this study used the AFN model to evaluate the impact of leakage orientation distribution on infiltration estimates. Using the Toronto climate, it was shown that annual space heating demand estimates increased up to 5% if the majority of envelope leakage faced up and downwind the dominate wind direction, and decreased up to 12% if it did not. This demonstrates that there could be appreciable energy performance implications if leakage location is taken into design considerations.

Using a more detailed approach to infiltration modelling, such as the method proposed here, may provide additional information to designers such as optimal placement of intentional openings to promote natural ventilation which cannot be modelled with AIM-2. The AFN method also enables the connection of mechanical ventilation systems for fully-coupled infiltration and ventilation simulation. However, the challenge is in defining the leakage site locations and characteristics of the façade. Spitler (2014) describes the crack method that may provide a useful first approach. Macdonald et al. (2020) previously compared this method to whole building field measurements of six commercial low and mid-rise commercial buildings and found good agreement.

Conclusions

The results of this study demonstrate that an AFN closely matches estimate building infiltration relative to an empirical validated model. It can provide improved estimates in the distribution of infiltration air to multi-zone small building models, capture the impacts of different leakage site elevations and orientations, and incorporate coupled ventilation systems. The challenge of using this method is the increased number of model inputs and assumptions required compared to established empirical methods. However, this paper demonstrated, how assumptions used in empirical methods may be adopted in AFN approaches to simplify model inputs.

Future Work

Future work will calibrate and validate the AFN of the IARL using empirical tracer gas measurements conducted at the site. As part of this work, a set of pressure coefficients reflective of the actual building geometry and surroundings will be developed both empirically and numerically. Future work will also explore detailed AFN modelling of attic space infiltration through soffits, vents, and cracks, as well as sensitivity to inter-zonal leakage modelling assumptions

References

Akins, R. E., Peterka, J. A., & Cermak, J. E. (1979). Averaged pressure coefficients for rectangular buildings. Proceedings of the Fifth International Wind Engineering Conference, (pp. 369-380). Fort Collins.

ASHRAE. (2014). ASHRAE Guideline 14: Measurement of Energy, Demand, and Water Savings. Atlanta: American Society of Heating, Refrigerating and Air-Conditioning Engineers.

Bradley, B., & Riley, M. (1993). Implementation of the AIM-2 Infiltration Model in HOT2000. Ottawa: Natural Resources Canada, CANMET-Ottawa.

Canadian Geographic. (2009). Canada's Wind Resource Map. Retrieved from Wind Energy | Canada's Wind TRM: https://www.nrcan.gc.ca/sites/www.nrcan.gc.ca/files/canmetenergy/pdf/fichier/81770/windtrm_resource_map.pdf

CCBFC. (2015). National Building Code of Canada. Ottawa: National Research Council of Canada.

CCBFC. (2017). National Energy Code of Canada for Buildings. Ottawa: National Research Council Canada, Codes Canada.

Clarke, J. A. (2001). Energy Simulation in Building Design (2nd ed.). Oxford: Butterworth-Heinemann.

Clarke, J. A. (2021). ESP-r. (Energy Systems Reseach Unit, University of Strathclyde) Retrieved January 27, 2022, from https://www.strath.ac.uk/research/energysystemsresearchunit/applications/esp-r/

ECCC. (2021). Engineering Climate Datasets. (Government of Canada) Retrieved May 31, 2018, from Environment and Climate Change Canada: https://climate.weather.gc.ca/prods_servs/engineering_e.html

Hensen, J. (1991). On the Thermal Interaction of Biuilding Structure and Heating and Ventilating System. Eindhoven: Technische Universiteit Eindhoven.

Macdonald, I., Bartko, M., Berquist, J., Wills, A., Banister, C., & Vuotari, M. (2020). Airtightness of Commercial Buildings - Measurement and Modelling Final Report. Ottawa: National Research Council Canada.

Sherman, M. H., & Grimsrud, D. T. (1980). Infiltration-Pressurization Correlation: Simplified Physical Modelling. Berkeley, CA: Lawrence Berkeley Laboratory, University of California.

Spitler, J. D. (2014). Load Calculation Applications Manual. Atlanta: American Society of Heating, Refrigerating and Air-Conditioning Engineers.

Walker, I., & Wilson, D. (1990). The Alberta Air Infiltration Model: AIM-2. Edmonton: University of Alberta, Department of Mechanical Engineering.